Temperature Wave-Trains of Periodically Forced Networks of Catalytic Reactors

Pietro Altimari
Dipartimento di Ingegneria Chimica e Alimentare, Università di Salerno, Via Ponte Don Melillo, 84084, Fisciano (SA), Italy

Erasmo Mancusi
Facoltà di Ingegneria, Università del Sannio, Piazza Roma, 82100, Benevento, Italy

Lucia Russo
CNR, Istituto di Ricerca sulla Combustione, P.le Tecchio 80, Napoli, 80125, Italy

Silvestro Crescitelli
Dipartimento d'Ingegneria Chimica, Università "Federico II" Piazzale Tecchio 80, I-80125 Napoli, Italy

DOI 10.1002/aic.12601
Published online March 22, 2011 in Wiley Online Library (wileyonlinelibrary.com).

Networks of N *identical catalytic reactors with periodically switched inlet and outlet sections are studied for first-order irreversible exothermic reactions. Switching strategies with inlet and outlet sections periodically jumping a fixed number* n_s *of reactors are considered and the mechanisms governing the formation of traveling temperature wave-trains are analyzed as* n_s *and* N *are varied. To this aim, a geometric approach to the analysis of the network energy balance is developed. Based on this approach, infinite domains of traveling temperature wave-trains are predicted for any* n_s *and* N*. Analytical approximations are derived for the stability limits and the spatiotemporal patterns of these regimes. Stability boundaries predicted analytically include for any solution the largest part of the stability region computed by numerical simulation. Moreover, good agreement is found between the structure of the spatiotemporal patterns computed numerically and that predicted based on the proposed approach.*
 AIChE J, 58: 899–913, 2012
Keywords: pattern formation, symmetric spatiotemporal patterns, periodically forced reactors, loop reactor, simulated moving bed, networks of reactors, temperature fronts, wave trains

Introduction

As the mechanisms of spontaneous pattern formation in extended systems are progressively understood,[1] an increasing number of studies is addressing the need to constructively interact with the building blocks of spatiotemporal patterns (pulses and waves) to design sustainable chemical process solutions.[2–4] A major objective is, in this context, to tailor the spatiotemporal pattern of catalytic reactors so as to optimize the temporal evolution of output variables as, for example, the conversion and the selectivity to a desired product.[5] A common approach followed to achieve this objective is to force reactor operating conditions. This is typically done by periodically varying reactor inputs and/or changing the location of the feed stream. The most representative example of application of the latter approach is the reverse-flow-reactor (RFR).[6] Here, inlet and outlet sections are periodically swapped leading to the inversion of the flow

Correspondence concerning this article should be addressed to P. Altimari at paltimar@unina.it and to E. Mancusi at mancusi@unina.it.

direction. When applied to catalytic exothermic processes, this operation mode enables to trap the exothermic reaction front within the catalytic bed preventing reactor shut-down even with streams characterized by very low adiabatic temperature rise. Numerical simulations have been also reported demonstrating the possibility to produce spatiotemporal patterns enhancing reaction yield and selectivity in equilibrium limited processes by appropriately controlling the switch time, that is the time after which the flow is reversed.[7]

The RFR exhibits, however, some drawbacks which are directly related to the inversion of the flow. The most important limit of such reactor solution is the washout effect, that is the lost of part of reactants immediately after the inversion. To overcome this limit, a network (NTW) of catalytic reactors equipped with a valve system allowing to modify inlet and outlet sections has been proposed.[6,8] With this system, autothermal operation of exothermic processes is achieved by periodically switching inlet and outlet sections so as to achieve a cyclic permutation of the NTW feed sequence while keeping constant the flow direction. In this way, the reaction front is still trapped within the bed, so as to avoid reactor shut-down, and, at the same time, the emission of unconverted reactants is prevented.[9] Also, periodically forced reactor NTWs have been proved to ensure a more uniform catalyst utilization than RFRs.[10,11] An experimental study has been also recently reported demonstrating the feasibility of the NTW operation mode for the catalytic combustion of ethylene.[12] This study has also shown the possibility to overcome technological difficulties related to the periodic switching of inlet and outlet ports by making use of an innovative valve system. However, complex dynamics can occur during the operation of forced reactor NTWs leading to severe controllability difficulties.

While the desired regimes of forced reactors NTWs are T-periodic, T being the period after which the NTW recovers the same feed sequence, such regimes have been proved to generally exhibit narrow ranges of stability. T-periodic regimes arise, for example, as the ratio of the switching to reaction front velocity is around unity.[13] The domain of existence of these regimes, whose boundaries can be analytically computed in terms of purely thermal and reaction front velocity,[13] becomes dramatically small as the adiabatic temperature rise and/or the feed temperature are decreased. Moreover, nT-periodic, quasi-periodic, and chaotic regimes can be likely detected as the ratio of the switching to thermal front velocity is increased.[14] It is also worth to remark that the NTW regimes may be symmetric or asymmetric as consequence of the spatiotemporal symmetry imposed by the switching strategy.[15]

Nonetheless, symmetric T-periodic regimes have been also shown to arise at switching to thermal front velocity ratios greater than unity[16] significantly extending the domain of operation of the forced NTW. These solutions give rise to trains of traveling temperature waves and exist within finger-like domains of the parameter space separated, at low adiabatic temperature rises, by domains of extinguished solutions. The analysis of these spatiotemporal patterns is of great practical relevance since for some parameter values the characteristics of the temperature profiles observed at switching to thermal velocity ratios around the unity might prevent safe operation. Under such conditions, the maximum bed temperature might for example exceed a threshold value imposed by the employed catalyst. In this case, larger switching to thermal velocity ratios corresponding to the formation of temperature wave trains must be selected. It must be also noted that temperature wave trains well reproduce the inter-stage cooling effect of multistage fixed bed reactors significantly increasing the average outlet conversion as equilibrium limited reactions are considered.[17]

Despite the practical relevance of these arguments, the physical mechanisms responsible for the emergence of travelling temperature wave trains remain still unclear. In particular, no general guidelines have been provided on how to approximately compute the stability limits of such regimes. These are rather detected by means of extensive numerical simulations.[16] Obviously, such an approach can likely fail to reveal the presence of periodic regimes characterized by narrow domains of stability.

It is also remarkable to note that most of the studies on the forced NTW have focused on the implementation of a unique switching strategy. Typically, inlet and outlet NTW sections are shifted in the flow direction so as to jump at switching a single reactor unit. Yet, an alternative switching strategy enabling to enlarge the switch time range of stability of ignited periodic regimes has been recently proposed.[18] Inlet and outlet NTW sections are here periodically shifted so as to jump a single reactor unit in direction opposite to the flow or, equivalently, N-1 reactor units in the direction of the flow, N being the number of reactors composing the NTW. The implementation of this strategy in the context of equilibrium limited reactions has been shown to allow for the formation of traveling temperature wave trains previously undetected.[17]

In this article, networks of N identical catalytic reactors with inlet and outlet sections periodically jumping n_s reactors in the flow direction are considered and the effects of varying n_s and N on the emergence of symmetric T-periodic regimes corresponding to travelling temperature wave trains are analyzed. To this aim, a pseudo homogeneous reactor model with first-order irreversible exothermic reaction is employed. The choice of this model is aimed at isolating the fundamental mechanisms driving the formation of temperature wave trains. With irreversible exothermic reactions, fresh reactants are indeed completely converted in a single reaction step giving rise to the formation of a unique reaction front travelling at constant velocity whereas multiple reaction fronts characterized by different velocities may form as equilibrium limited reactions are analyzed.[17] In this framework, a geometric approach to the analysis of the NTW energy balance is developed. Following this approach, infinite domains of travelling temperature wave trains are predicted for any n_s and N. Moreover, analytical relationships are derived for stability limits and the structure of temperature wave trains in terms of switching, purely thermal and reaction front velocity.

The rest of the article is structured as follows. First, the mathematical model of the forced NTW is described. Then, the main elements characterizing the interaction of traveling reaction and purely thermal fronts with periodically switched inlet and outlet sections are described. Particularly, a geometric approach to the analysis of the NTW energy balance is presented. Based on this approach, analytical relationships are successively derived for the spatiotemporal patterns and the stability limits of symmetric T-periodic regimes

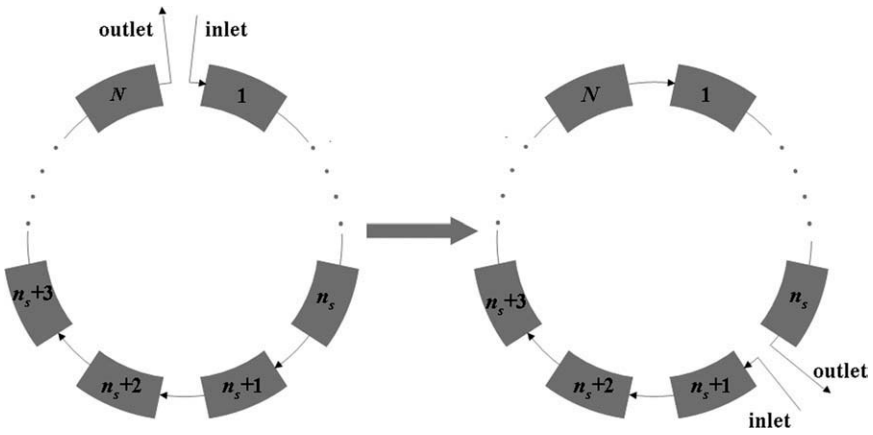

Figure 1. Schematic representation of the forced NTW. Inlet and outlet sections are rotated at each switching instant so as to jump n_s reactor units.

corresponding to traveling temperature wave-trains. Comparison between analytical predictions and numerical simulations is then shown. Final remarks complete the article.

Mathematical Model

In this section, the mathematical model of the forced NTW is presented. In particular, the class of switching strategies considered in this work is described and model equations are presented.

Switching strategies

We consider NTW of connected N identical fixed-bed catalytic reactors organized in a loop (see Figure 1 for a representative scheme). Inlet and outlet NTW sections are stepwise periodically rotated in the flow direction so as to jump n_s reactor units at each switching instant. We refer to the period between two consecutive switches as the switch time (or cycle) τ and define the switching velocity as $V_{sw} = n_s/\tau$.

$N-1$ switching strategies can be identified as n_s varies over the set $\{1 \ldots N-1\}$. An example is reported in Figure 2a for $N = 4$ and $n_s = 3$. It can be here noted that the NTW recovers the initial feed sequence after a number of switches exactly equal to the number of reactors composing the NTW, that is $N = 4$. This rule holds however if and only if n_s and N are coprime. As shown in Figure 2b, the NTW recovers, for example, the initial feed sequence after only two switches when $N = 4$ and $n_s = 2$. It can be also observed that the NTW behaves, in this case, as composed of $N' = 2$ reactors, each resulting from sequence of two actual reactor units, switched with $n'_s = 1$. The results obtained by analyzing these examples can be readily generalized to any n_s and N. It can be, in particular, proved that the NTW recovers the initial feed sequence after a number of switches $N' = N/gcd(N, n_s)$, $gcd(N, n_s)$ being the greatest common divisor of N and n_s. Moreover, if N and n_s have common divisors greater than the unity, the NTW behaves as composed of N' reactors, each resulting from the sequence of $gcd(N, n_s)$ actual reactor units, switched with $n'_s = n_s/gcd(N, n_s)$. Therefore, we only consider in this article coprime values for N and n_s.

Model equations

We restrict our analysis to first-order exothermic irreversible reactions and assume constant physical properties and negligible inter-phase gradients. Under these assumptions, mass and energy balances for the ith reactor unit can be written as follows:

$$\frac{\partial x_i}{\partial \bar{t}} + v\frac{\partial x_i}{\partial \xi} = \frac{1}{Pe_m}\frac{\partial^2 x_i}{\partial \xi^2} + Da(1-x)\exp\left(\frac{\vartheta_i \gamma}{\vartheta_i + \gamma}\right)$$
$$Le\frac{\partial \vartheta_i}{\partial \bar{t}} + v\frac{\partial \vartheta_i}{\partial \xi} = \frac{1}{Pe_h}\frac{\partial^2 \vartheta_i}{\partial \xi^2} + BDa(1-x)\exp\left(\frac{\vartheta_i \gamma}{\vartheta_i + \gamma}\right) \quad (1)$$

with the following definitions for dimensionless variables and parameters:

$$\xi = \frac{z}{L}; \bar{t} = \frac{tu_0}{L}; \vartheta = \gamma\frac{T - T_0}{T}; x = 1 - \frac{C}{C_0}; \gamma = \frac{E}{RT_0};$$
$$v = \frac{u}{u_0}; B = \frac{(-\Delta H)C_0\gamma}{(\rho c_p)_f T_0}; Da = \frac{AL}{u_o}\exp(-\gamma); Le\frac{(\rho c_p)_{\text{eff}}}{(\rho c_p)_f};$$
$$Pe_h = \frac{(\rho c_p)_f Lu_o}{k_e}; Pe_m = \frac{(\rho c_p)_f Lu_o}{D_f}. \quad (2)$$

where L denotes the length of a single reactor unit. Danckwerts boundary conditions are applied at inlet and outlet sections of each reactor and are modified after each cycle to take into account the permutation of the NTW feed sequence. In particular, dimensionless boundary conditions can be written as follows:

$$\frac{1}{Pe_m}\frac{\partial x_i}{\partial \xi}\bigg|_0 = -[1 - f_i(t)]\theta_{in} - f_i(t)\theta_{i-1}(i-1,t) + \theta_i(i-1,t)$$
$$\frac{1}{Pe_h}\frac{\partial \theta_i}{\partial \xi}\bigg|_0 = -[1 - f_i(t)]\theta_{in} - f_i(t)\theta_{i-1}(i-1,t) + \theta_i(i-1,t)$$
$$\frac{\partial x_i}{\partial \xi}\bigg|_1 = \frac{\partial \theta_i}{\partial \xi}\bigg|_1 = 0 \quad (3)$$

where $f_i(t) = g\,(t - mod((i-1)n_s, N)\,\tau$ with $mod(*,\cdot)$ denoting the standard modulo function[19] and $g(t)$ describing the following step-wise constant periodic function:

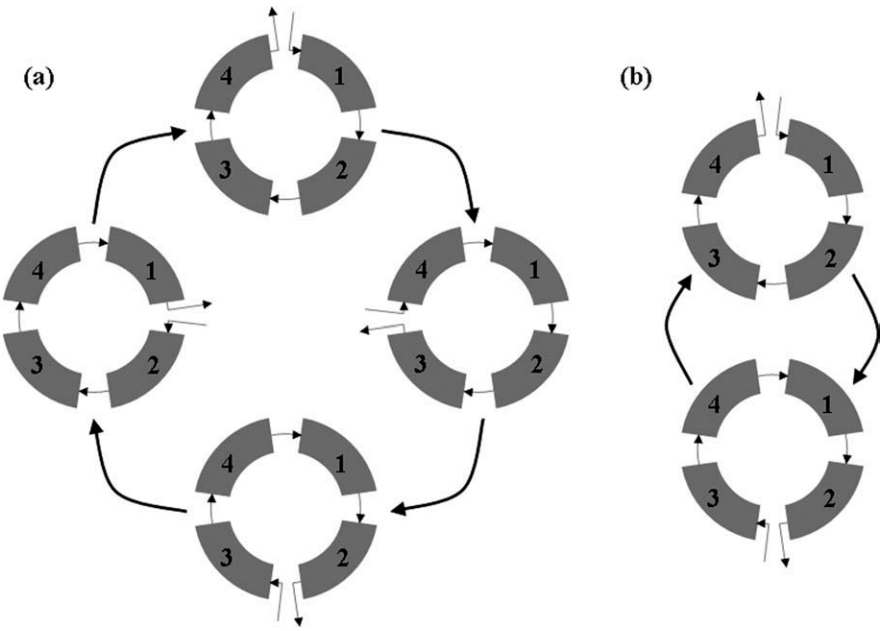

Figure 2. Evolution of the NTW sequence. (a) $n_s = 3$ and $N = 4$; (b) $n_s = 2$ and $N = 4$.

$$g(t) = \begin{cases} 0 & \text{if } 0 \le mod\left(\frac{t}{\tau}, N\right) < 1 \\ 1 & \text{if } mod\left(\frac{t}{\tau}, N\right) > 1 \end{cases} \quad (4)$$

It should be emphasized that the governing equations of the forced NTW with different n_s values only differ from a mathematical standpoint by the way the forcing function $g(t)$ enters the boundary conditions (3).

Results presented in this article are obtained, unless otherwise specified, with parameter values reported in Table 1. It is worth to note that a constant length L_0 for the NTW is used independently of the selected N. Therefore, Peclet and Damkohler number values reported in Table 1 are scaled by N to account for the dependence of the length L of a single reactor unit on N. In any case, only parameter values at which the unforced system does not exhibit ignited regimes are considered. Under such conditions, the forced NTW only exhibits ignited regimes corresponding to almost complete conversion of the reactants and non-ignited regimes characterized by very low conversion values.

Two examples of T-periodic regimes predicted with $n_s = 3$, $N = 4$ and reactor parameter values reported in Table 1 are described in Figure 3. Temperature profiles observed at two instants of a given cycle and grey scale spatiotemporal temperature patterns are presented in Figure 3a,b and Figure 3c,d respectively. It is important to note that the dimensionless time t^* is scaled in Figure 3c,d by the switch time τ. As a result, each cycle is here identified by a unit interval of variation of t^*/τ. Vertical bold lines are also used in Figure 3c,d to denote the position kept during each cycle by inlet and outlet sections. The considered regimes are symmetric as the corresponding spatiotemporal patterns repeat unchanged during each cycle provided that the sequence of reactor units is appropriately permutated.[15] Moreover, they give rise to sequences (or trains) of temperature waves travelling over the catalytic bed in the flow direction. Each temperature wave results from a hot bed region delimitated by two temperature fronts and separates two consecutive cold bed regions. This leads to the alternation of dark and light grey stripes moving from the left to the right over the grey-scale spatiotemporal temperature pattern. Particularly, light grey stripes correspond to moving hot bed regions and are separated from each other by dark grey stripes denoting cold bed regions. The border lines delimitating these stripes identify temperature fronts. Therefore, the velocity of each temperature front can be evaluated as inverse of the product between the switch time τ and the slope of the straight line separating the adjacent cold and hot bed regions.[18] The need to multiply the slope of the line by τ is here a consequence of scaling t^* by τ. It is apparent that all the observed temperature fronts move with almost constant velocity during each cycle with the only exception of a transient immediately following the switching instant. This transient is however much shorter than any switch time τ of practical relevance. Therefore, it is assumed throughout the paper that each temperature front moves at constant velocity.

Traveling Temperature Fronts and NTW Energy Balance

As apparent from Figure 3, NTW operation exploits the ability of catalytic beds to develop traveling temperature fronts. In particular, the periodic variation of the NTW feed sequence enables to trap an exothermic reaction front within the system. This mechanism allows, for example, autothermal operation at switching velocity values around the velocity of a purely thermal front[13]. In this section, spatiotemporal patterns arising under such conditions are analyzed with the objective of illustrating the main physical mechanisms governing the formation of temperature and conversion patterns. As an example, we describe in Figure 4a the formation of a

Table 1. Dimensionless Parameter Values

Damkohler number, Da	$0.0129/N$
Dimensionless activation energy, γ	14.13
Dimensionless adiabatic temperature rise, B	10.28
Dimensionless feed temperature, θ_{in} (corresponding to $T_{in} = 100°C$)	−4.82
Dimensionless velocity, v	1
Lewis number, Le	800
Peclet number for heat conduction, Pe_h	$312.5/N$
Peclet number for mass diffusion, Pe_m	$500/N$

Dimensional parameter values $u_0 = 0.5$ m/s, $L_0 = 0.5$ m, $C_0 = 1e-3$ kmol/m^3, $T_0 = 293°C$ are employed.

symmetric T-periodic spatiotemporal temperature pattern arising with $N = 4$ and $n_s = 3$ at $\tau = 2450$ starting from uniform initial conditions $T(z,0) = 1600°C$ and $x(z,0) = 0$. A grey-scale spatiotemporal pattern describing the evolution of the temperature profile is reported in Figure 4a while snapshots providing a detailed description of the temperature profile are reported in Figure 4b.

Under conditions corresponding to Figure 4, fresh reactants are fed to reactor 1 at $t^* = 0$. Since the bed is initially completely hot, a reaction front forms near the inlet section of reactor 1 and moves at constant dimensionless velocity V_{fr} slightly greater than the reciprocal of the Lewis number $1/Le$.[20] The motion of the reaction front is described by the straight line separating over the spatiotemporal temperature pattern (Figure 4a) the upstream cold region from the downstream hot one. This line describes the position kept by the reaction front at any instant of the considered cycle and will be referred to as the spatiotemporal path followed by the reaction front. As a result of the displacement of the reaction front, the upstream bed region is progressively cooled. In particular, the initial three reactors are almost completely cold at the end of the first cycle since the ratio of the reaction front velocity $V_{fr} \sim 1/Le = 1/800$ to the selected switching velocity $V_{sw} = n_s/\tau = 3/2450$ is around the unity. Inlet and outlet NTW sections are then switched so as to jump $n_s = 3$ reactor units. Accordingly, fresh reactants are fed to reactor 4 which is still completely hot. Therefore, a new reaction front forms near the inlet section of reactor 4 after switching. The heat released by the reaction is now transferred by thermal convection to the part of the bed left cold by the displacement of the reaction front during the first cycle. In particular, a purely thermal front arises near the inlet section of reactor 1 and moves at constant velocity $V_{th} = 1/Le$. This front transfers the reaction heat to the downstream cold region. Also, a purely thermal front forms immediately after switching close to the outlet section of reactor 3 and cools the part of such reactor uncovered by the reaction front during the first cycle. The motion of the two formed purely thermal fronts is again described over the spatiotemporal pattern by two straight lines delimitating cold and hot bed regions. These lines can be easily distinguished since they are characterized by slope lower than that found for the reaction front and will be referred to as spatiotemporal paths followed by the purely thermal fronts.

As a result of the periodic switching of inlet and outlet sections, a reaction and two purely thermal fronts are found to form at the beginning of each following cycle. Particularly, an upstream cold region is generated during each cycle by the displacement of the reaction front while the reaction

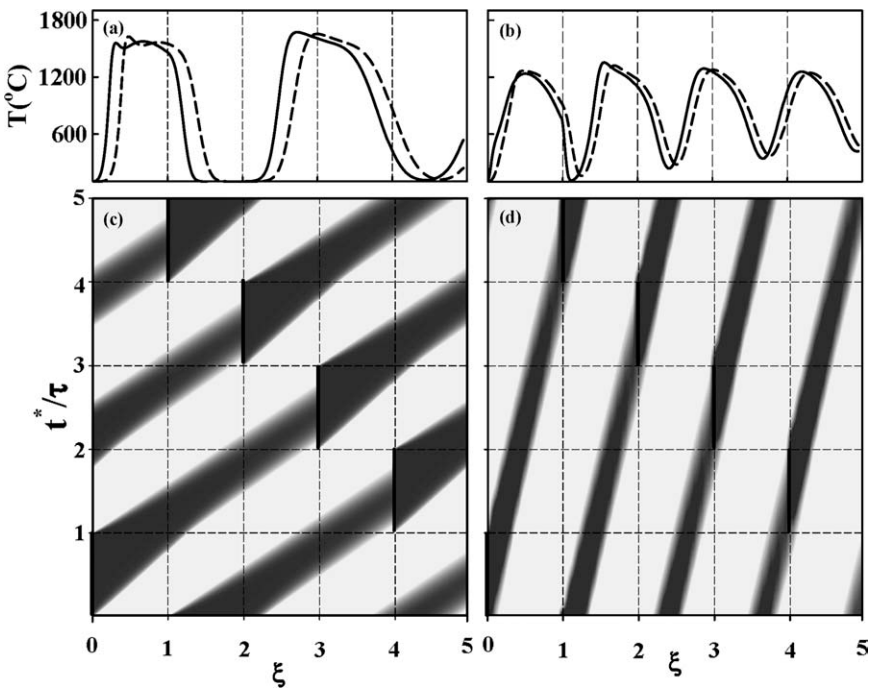

Figure 3. Symmetric *T*-periodic regimes corresponding to travelling temperature wave trains observed at $\tau = 1300$ ((a), (c)) and $\tau = 210$ ((b), (d)) with $n_s = 3$ and $N = 5$; (a), (b) temperature profiles observed at two instants of the cycle; ((b), (d)) grey-scale spatiotemporal temperature patterns (dark and light grey corresponds to cold and hot regions respectively while vertical bold lines denote the position kept by inlet and outlet section during each cycle).

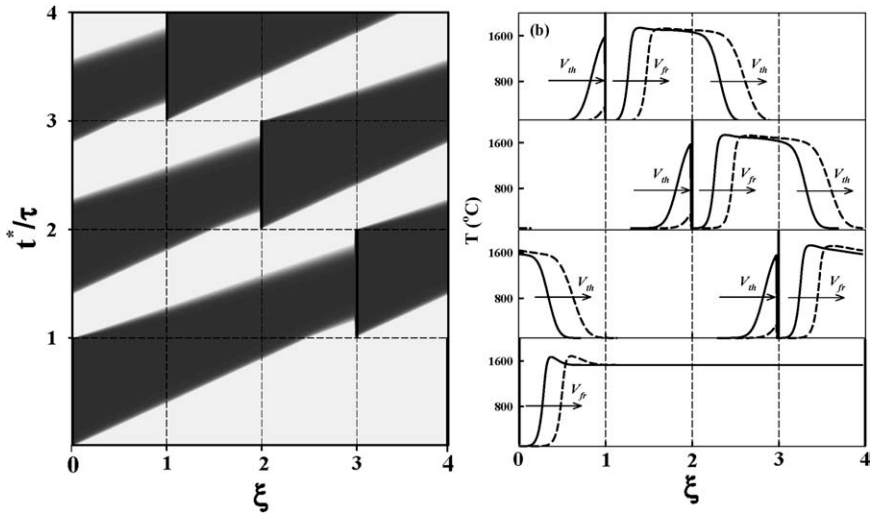

Figure 4. Formation of a symmetric *T*-periodic spatiotemporal temperature pattern with $N = 4$ and $n_s = 3$ at $\tau = 2450$ starting from uniform initial conditions $T(z,0) = 1700°C$ and $x(z,0) = 0$; (a) grey-scale spatiotemporal temperature pattern; (b) temperature profiles observed at two instants of each cycle (arrows indicate the moving direction of the temperature fronts while superscripts V_{fr} and V_{th} are used to denote reaction and purely thermal fronts respectively).

heat is transferred to the downstream bed region by two purely thermal fronts. To ensure the fulfillment of the energy balance within a single cycle, the reduction in the enthalpy of the bed caused by the displacement of the reaction front must be therefore equal to the enthalpy overall transferred to the bed by purely thermal fronts. This balance is established under conditions of Figure 4 where a symmetric *T*-periodic regime is achieved after about four cycles. For the sake of clarity, we separately report in Figure 5 the spatiotemporal temperature pattern corresponding to this regime. It is here apparent that while the reaction front generates during each cycle a cold region of length $V_{fr}\tau$, a purely thermal front heating 3 reactors and a purely thermal front cooling a part of the bed of length $3\text{-}V_{fr}\tau$ are found. This enables to fulfill the network energy balance within a single cycle giving rise to the formation of the rectangular-like temperature wave displayed in Figure 5b. This temperature wave is delimitated upstream by the reaction front and downstream by a purely thermal front and, hence, exhibits width increasing during the cycle since $V_{fr} < V_{th}$. The corresponding conversion profiles are also reported in Figure 5c. A step-like conversion front traveling at velocity V_{fr} is observed since almost complete conversion is achieved over a narrow region around the reaction front.

The way autothermal NTW operation is established under regime conditions described in Figure 5 is susceptible of a geometric interpretation. To show it, we draw attention to the points F_1 and F_2 of Figure 5 delimitating, at switching, the cold region of length $V_{fr}\tau$ generated by the displacement of the reaction front during the previous cycle. Starting from these points, two purely thermal fronts form and move over the bed at velocity V_{th}. As a result, the region $\overline{F_1F_2}$ is shifted unchanged downstream until the two purely thermal fronts reach the NTW outlet section and then leaves the NTW. Therefore, a cold region $\overline{F_1F_2}$ is simultaneously generated and swept away from the NTW during each cycle due to the displacement of reaction and purely thermal fronts respectively. Variations in τ can however produce the impossibility for the purely thermal fronts forming at F_1 and F_2 to reach the NTW outlet section within a single cycle. Since t^* is scaled by τ, variations in τ produce indeed in Figure 5a modification in the slope of the spatiotemporal paths followed by reaction and purely thermal fronts. Particularly, the slope of such paths proportionally decrease with τ. An increase in τ can, for example, cause the reaction front to cross the inlet section of the third reactor. This situation occurs when the reaction front covers during a single cycle a region of length greater than 3, that is $V_{fr}\tau > 3$. If such switch time values are selected, the reaction front moves faster than the NTW outlet section and eventually reaches it causing reaction extinction. This effect is illustrated in Figure 6a. We here report the spatiotemporal temperature pattern computed with a switch time value greater than $3/V_{fr}$ starting from the solution regime described in Figure 5. A clockwise rotation of the spatiotemporal paths followed by reaction and purely thermal fronts is observed compared with Figure 5. To clearly show it, we also display in Figure 6a the spatiotemporal paths followed by reaction and purely thermal fronts during the first cycle of Figure 5. The increase in τ causes the reaction front to lie at the beginning of the second cycle downstream to the reactor inlet section. As a consequence, the reaction front is formed at the beginning of each following cycle at sections progressively farther from the NTW inlet section determining after few cycles the complete cooling of the bed. It can be analogously verified that the purely thermal front forming in F_1 cannot reach the NTW outlet section within a single cycle if $V_{th}\tau < 3$. Under these conditions, the purely thermal fronts forming in F_1 and F_2 cannot warm within a single cycle the cold region generated by the displacement of the reaction front. Particularly, only part of the cold region $\overline{F_1F_2}$ is swept away from the NTW. To show it, we report in Figure 6b the spatiotemporal temperature pattern computed with a switch time value lower than $3/V_{th}$ starting from the solution regime described in Figure 5. A

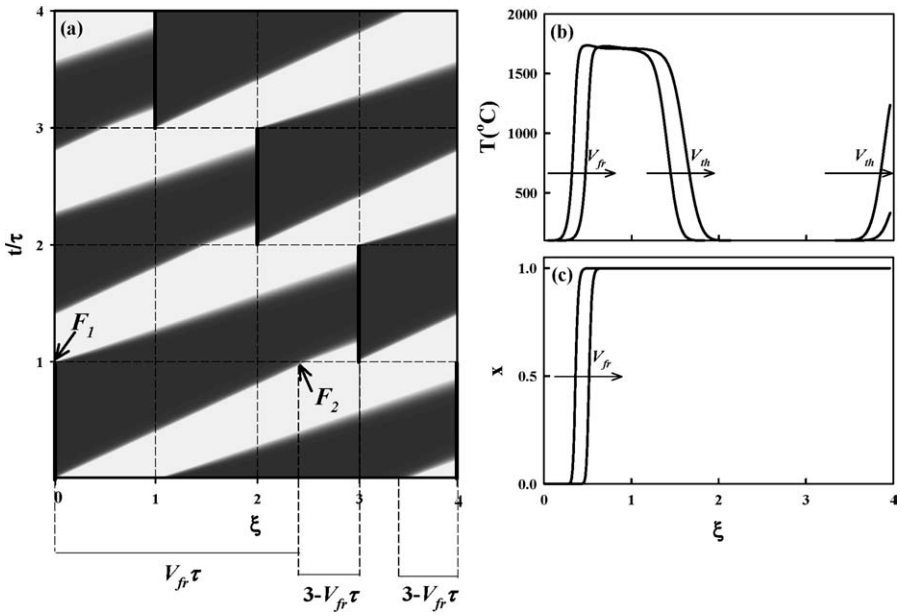

Figure 5. Symmetric *T*-periodic regime observed with $n_s = 3$ and $N = 4$ at $\tau = 2450$; (a) grey-scale spatiotemporal temperature pattern; (b), (c) temperature and conversion profiles predicted at two instants of the cycle respectively.

counterclockwise rotation of the spatiotemporal paths followed by reaction and purely thermal fronts is observed compared to Figure 5 as consequence of the reduction in τ. A cold region exhibiting width progressively increasing is therefore found. This eventually leads to the complete cooling of the bed.

The previous results can be readily extended to any N and n_s. It can be, in particular, shown based on similar arguments that symmetric T-periodic regimes always arise, as N and n_s are varied, at switch time values $\tau \in [n_s/V_{th}, n_s/V_{fr}]$. This switch time range corresponds to switching velocity values $V_{sw} \in [V_{fr}, V_{th}]$. Periodic regimes detected under these conditions give rise to single traveling temperature waves extending to about $N - n_s$ reactor units.

Temperature Wave-trains: Stability Limits and Structure

In this section, the mechanisms governing the formation of symmetric T-periodic regimes corresponding to trains of travelling temperature waves are analyzed. The starting point is the geometric based analysis of the NTW energy balance illustrated in the previous section. Based on this approach, infinite domains of traveling temperature wave-trains are predicted for any n_s and N. Analytical relationships for the stability limits of these regimes are derived. Then, an algorithm to get a description for the structure of the corresponding spatiotemporal temperature and conversion patterns is outlined.

Structure of the operating domains

In accordance with the analysis presented in the previous section, the balance between the reduction in the enthalpy of the bed caused by the displacement of the reaction front and the reaction heat transferred to the bed by thermal convection can be imposed by requiring that the two purely thermal fronts forming at F_1 and F_2 reach the NTW outlet section within a single cycle. This condition enables however to identify a class of infinite and not just a single periodic regime. To verify it, it is sufficient to relax the condition on the number of cycles needed for the fronts forming at F_1 and F_2 to reach the NTW outlet section. This number ranges between zero and one in Figure 5. Decreasing τ produces however a counterclockwise rotation of the spatiotemporal paths followed by reaction and purely thermal fronts making possible for the two purely thermal fronts forming at F_1 and F_2 to reach the NTW outlet section after a number of cycles greater than one. To show it, we qualitatively describe in Figure 7a the spatiotemporal paths of reaction and purely thermal fronts derived from Figure 5 by gradually decreasing the switch time to $\tau \sim 1/V_{th}$, and $\tau \sim 1/(3V_{th})$. For the sake of clarity, only the paths of the reaction front forming at $t^*/\tau = 0$ and of the purely thermal fronts forming at $t^*/\tau = 1$ are here reported. We remark however that the complete description of the NTW spatiotemporal temperature pattern would impose to replicate such construction over each following cycle.

In the two cases considered in Figure 7a (dashed and dashed-dotted lines), the two purely thermal fronts forming at F_1 and F_2 reach the NTW outlet section after two and three cycles respectively. It is however sufficient to draw the paths followed by reaction and purely thermal fronts forming at each following switching instant to verify that the NTW energy balance is still fulfilled within a single cycle. This clearly appears from Figure 7b where the spatiotemporal temperature pattern computed by numerical simulation at $\tau \sim 1/V_{th}$ is reported as representative example. A cold region $\overline{F_1F_2}$ is simultaneously generated and swept away from the NTW during each cycle due to the displacement of reaction

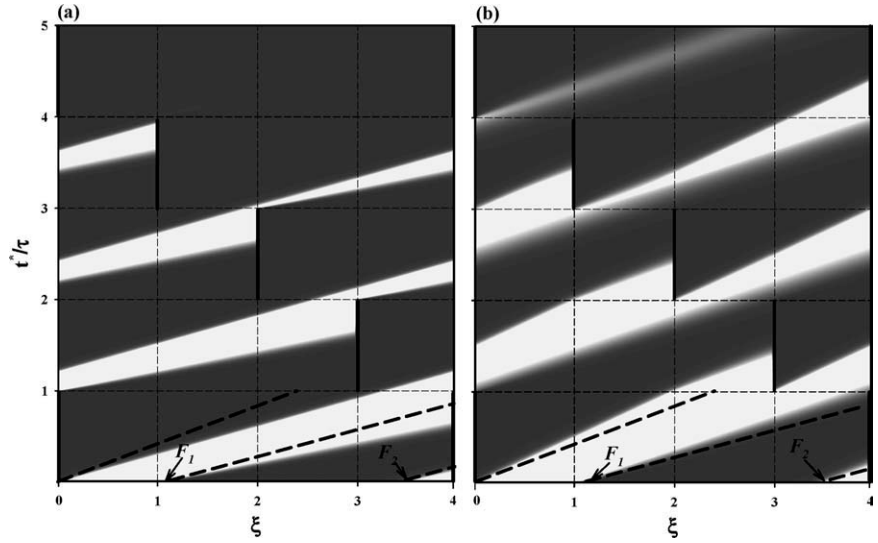

Figure 6. Grey-scale spatiotemporal patterns illustrating the extinction of the temperature wave described in Figure-5a as consequence of a step-change to (a) $\tau = 3500$ and (b) $\tau = 2100$ (bold dashed lines describe the spatiotemporal paths followed by reaction and purely thermal fronts in Figure 5); (a) the increase in τ determines a clockwise rotation of the spatiotemporal paths followed by reaction and purely thermal fronts causing the reaction front to form at section progressively farther from the NTW inlet section; (b) the reduction of τ produces a clockwise rotation of the spatiotemporal paths followed by purely thermal fronts causing the impossibility for the purely thermal front forming in F_1 to reach the NTW outlet section within a single cycle.

and purely thermal fronts respectively. However, since about two cycles are needed for the purely thermal fronts forming at F_1 and F_2 to reach the NTW outlet section, the bed is now crossed during each cycle by two distinct cold regions $\overline{F_1F_2}$ generated by the reaction front during the previous two cycles. As a result, four purely thermal fronts are simultaneously found to move over the bed. In addition, a reaction front always forms at switching near the NTW inlet section and moves over the bed during the following cycle. Therefore, the sequence of a reaction and four purely thermal fronts is found. This gives rise to the train of two travelling temperature waves shown in Figure 7c. It is worth to note that while the upstream temperature wave delimitated by the reaction and the following purely thermal front exhibits width increasing since $V_{fr} < V_{th}$, the second temperature wave shows on the contrary almost constant width since it is delimitated by only purely thermal fronts travelling at velocity V_{th}. We also report in Figure 7d the corresponding conversion profiles. A single step-like conversion front traveling over the catalytic bed at velocity V_{fr} is found since the reactants are again almost completely converted over narrow region around the reaction front.

It is now possible to derive an approximation for the switch time range of stability of spatiotemporal patterns of the type described in Figure 7b. The time needed for the purely thermal fronts forming at F_1 and F_2 to reach the NTW outlet section varies for these patterns between one and two cycles. This condition can be fulfilled only with switch time values greater than $1/V_{th} = Le$. With this switch time, the thermal front forming at F_1 indeed reaches the NTW outlet section within exactly two cycles (see dashed line in Figure 7b). Similarly, it can be checked that the maximum switch time value enabling the formation of spatiotemporal patterns of the type described in Figure 7b must fulfill the equality $2 - V_{th}\tau = V_{fr}\tau$. This relationship can be derived by imposing that the purely thermal front forming in F_2 takes one cycle to reach the NTW outlet section (see dashed-dotted lines in Figure 7b).

Similar arguments can be followed to compute the switch time values sustaining the formation of any spatiotemporal pattern derived by further rotating the spatiotemporal paths followed by reaction and purely thermal fronts. Particularly, the previous results can be extended to any n_s and N. To this aim, it is sufficient to note that the dimensionless axial position of the NTW outlet section initially fixed at $q = q_0$ becomes $q = mod(n_s\ k + q_0, N)$ after k switches and does not change during the following cycle. Then, simple kinematics rules can be applied to compute the switch time ranges of stability of the predicted patterns as n_s and N vary. A schematic representation illustrating how these rules apply in the general case is shown in Figure 8.

It is here assumed that purely thermal fronts take between $(p - 1)$ and p cycles to reach the NTW outlet section. Under these conditions, a cold region $\overline{F_1F_2}$ is generated during each cycle by the displacement of the reaction front and then shifted downstream during the following p cycles before reaching the NTW outlet section. Hence, p distinct cold regions $\overline{F_1F_2}$, or equivalently $2p$ purely thermal fronts, are found travelling over the catalytic bed during each cycle. In addition a reaction front forms at each switching instant near the NTW inlet section and moves over the bed at

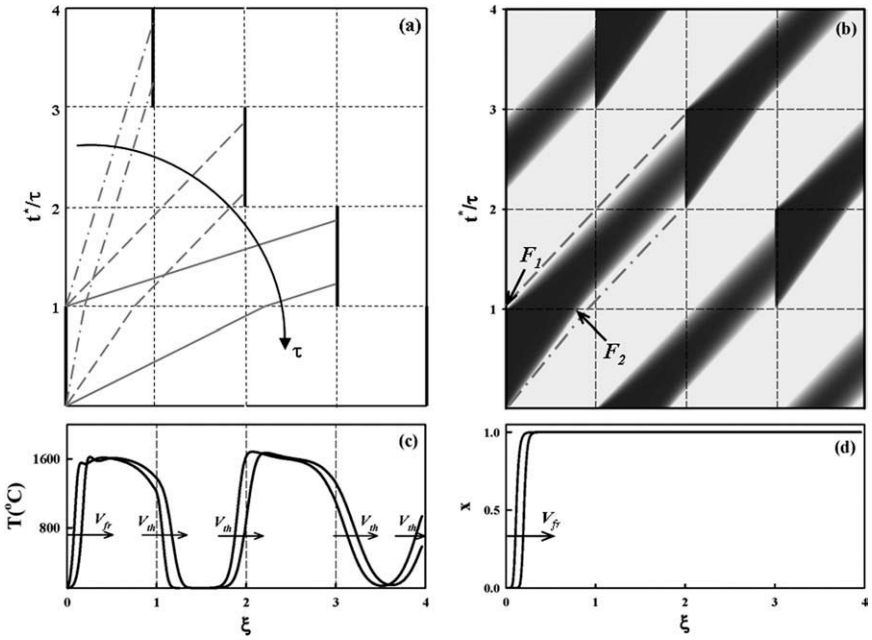

Figure 7. Formation of temperature wave-trains from single temperature waves observed at $V_{sw}/V_{th} \sim 1$; (a) three different ways of the purely thermal fronts forming in F_1 and F_2 to intercept the NTW outlet section during the same cycle as τ varies; (b), (c), (d) spatiotemporal temperature pattern, temperature and conversion profiles corresponding to the symmetric *T*-periodic regime computed at $\tau = 850$, respectively.

constant velocity. This gives rise to the formation of a train of p travelling temperature waves. Figure 8a shows that the minimum switch time sustaining the formation of such spatiotemporal patterns fulfills the following inequality:

$$V_{th}p\tau - mod(n_s p, N) \geq 0 \tag{6}$$

that solved in τ gives:

$$\tau \geq \frac{mod(n_s p, N)}{V_{th}p} \tag{7}$$

Also, the following condition can be derived from Figure 8b for the upper switch time limit:

$$mod(n_s p, N) - V_{th}(p-1)\tau \geq V_{fr}\tau \tag{8}$$

that solved in τ gives:

$$\tau \leq \frac{mod(n_s p, N)}{V_{fr} + V_{th}(p-1)} \tag{9}$$

Therefore, the following switch time ranges of existence are found:

$$\frac{mod(n_s p, N)}{V_{th}p} \leq \tau \leq \frac{mod(n_s p, N)}{V_{fr} + V_{th}(p-1)} \tag{10}$$

When an explicit expression for the dependence of the reaction front velocity V_{fr} on reactors parameters is available,[20] inequalities (10) can be employed to rapidly compute an approximation for the stability limits of the predicted spatiotemporal patterns. It is worth to note that inequalities (10) give with $p = 1$ the switch time ranges of existence of symmetric T-periodic regimes corresponding to a single temperature waves of the type described in Figure 5.

The limits of existence of the predicted patterns can be also expressed in terms of the switching velocity by substituting the expression $\tau = n_s / V_{sw}$·in (10). This gives:

$$\frac{mod(n_s p, N)}{n_s p} \leq \frac{V_{th}}{V_{sw}} \leq \frac{mod(n_s p, N)}{n_s\left(\frac{V_{fr}}{V_{th}} + p - 1\right)} \tag{11}$$

Since the ratio V_{fr}/V_{th} is generally slightly greater than the unity, it can be concluded, based on (11), that spatiotemporal patterns characterized by temperature wave trains always arise at purely thermal front to switching velocity ratios $V_{th}/V_{sw} \cong mod(n_s{\cdot}p, N)/(n_s{\cdot}p)$, p being a positive integer.

Approximate description of the spatiotemporal patterns

The number p of cycles needed for the purely thermal fronts forming at F_1 and F_2 to reach the NTW outlet section completely characterizes the structure of the predicted spatiotemporal patterns. p distinct cold regions of length $V_{fr}\tau$ traveling at velocity V_{th} are indeed found during each cycle. In addition, a cold region of increasing width following the NTW inlet section is generated during each cycle by the displacement of the reaction front. Based on this scheme, we derive in Figure 9 the structure of the spatiotemporal temperature pattern observed with $n_s = 3$ and $N = 5$ at switch time

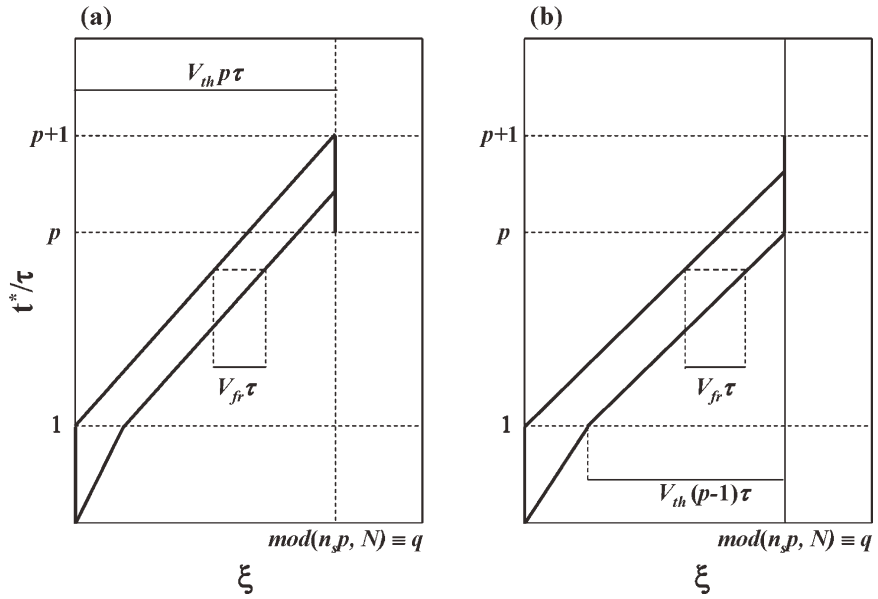

Figure 8. Schematic representation of the NTW spatiotemporal temperature pattern illustrating how to derive the stability limits of symmetric *T*-periodic regimes corresponding to temperature wave trains.

values fulfilling (10) with $p = 3$. It is shown that the spatiotemporal temperature pattern corresponding to the fourth cycle can be derived by just drawing the paths followed by the purely thermal fronts formed at the initial three switching instants and by the reaction front forming near the NTW inlet section.

Figure 9a,c suggest a general procedure to derive an approximate description for the structure of the NTW temperature profile. This profile can be roughly described by a train of rectangle waves delimitated by reaction and purely thermal fronts. These rectangular waves are uniquely defined at any instant by the axial positions of reaction and purely thermal fronts. Since reaction and purely thermal fronts move at constant velocities V_{fr} and V_{th}, their axial positions at $t^* \in [(k\tau, (k + 1)\tau]$ can be computed by shifting the axial positions at $t^* = k\tau$ by $V_{fr}(t^* - k\tau)$ and $V_{th}(t^* - k\tau)$, respectively. To this aim, it is sufficient to compute the axial positions of purely thermal fronts at switching, that is at $t^* = k\tau$, since the reaction front always forms immediately after the NTW inlet section. As shown in Figure 9a for the case $n_s = 3$, $N = 5$ and $p = 3$, such axial positions can be found by drawing the paths followed by the purely thermal fronts formed at the previous p switching instants. A rigorous formulation of the algorithm to be implemented to get a rectangular wave-train approximation of the NTW temperature profile is reported in appendix.

The spatiotemporal temperature pattern derived in Figure 9a,c arises, in accordance with (10), at switch time values $\tau \in [4/(3V_{th}), 4/(2V_{th}+V_{fr})]$. Such range corresponds, with the employed parameter values, to $\tau \in [1066, 1118]$. Therefore, we show in Figure 9d the spatiotemporal temperature pattern computed by numerical simulation at $\tau = 1100$. It is apparent that the schematic representation reported in Figure 9c satisfactorily describes the structure of the pattern displayed in Figure 9d. The NTW temperature profile observed at a given instant of the fourth cycle under conditions corresponding to Figure 9d is also compared with the train of rectangular waves derived by implementation of the proposed algorithm in Figure 9b. Although not reported in Figure 9, it is worth to note that the evolution of the NTW conversion profile during a given cycle can be also approximated to a unit step function forming immediately after the NTW inlet section and moving over the catalytic bed at constant velocity V_{fr}.

Remark 1

Results of parametric continuation of symmetric *T*-periodic regimes corresponding to travelling temperature wave trains show that the derived switch time limits (10) correspond to limit point bifurcations. This is in line with previous studies showing that the domain of existence of spatiotemporal patterns arising at switching to thermal velocity ratios around unity is also delimitated by limit point bifurcations.[20] A detailed characterization of the bifurcation characteristics of the NTW deserves, however, to be further investigated. Particularly, the influence of thermal dispersion on the stability characteristics of travelling temperature wave trains arising at low switch time values should be thoroughly analyzed. As τ is decreased, the width $V_{fr}\tau$ of the cold region $\overline{F_1F_2}$ becomes indeed progressively smaller making reaction and purely thermal fronts travelling over the catalytic bed to approach each other. Under these conditions, it may be no longer possible to distinguish between consecutive hot and cold bed regions making necessary to revise the presented analysis. This goes, however, beyond the scope of the paper and will be the subject of future work.

Remark 2

In accordance with the illustrated analysis, traveling temperature wave trains are always detected, for any n_s, N, and p, at switch time values fulfilling (10). However, while inequalities (10) necessarily hold when purely thermal fronts reach the NTW outlet section between $(p - 1)$ and p cycles,

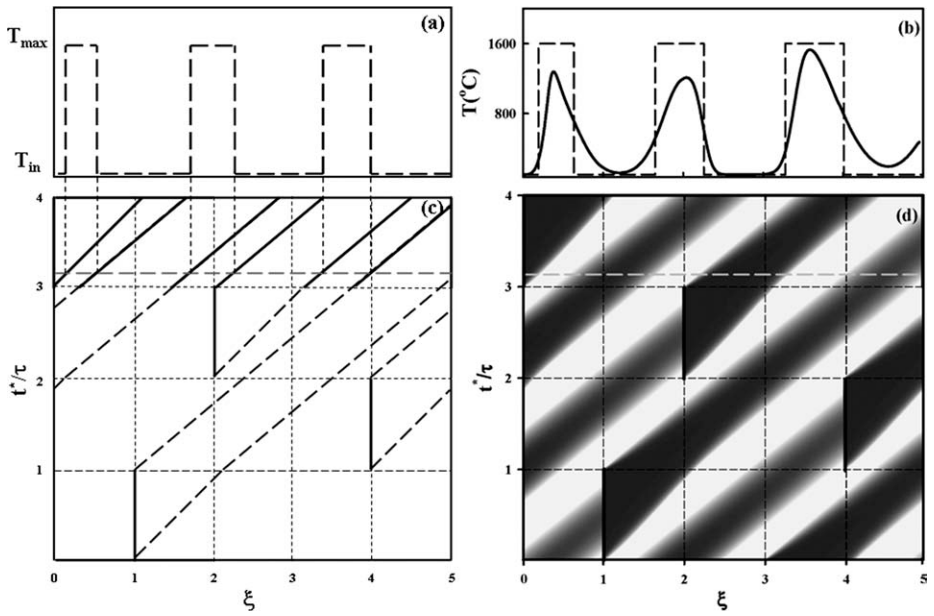

Figure 9. Approximation of a train of three temperature waves observed with $n_s = 3$ and $N = 5$.

The spatiotemporal paths followed by purely thermal fronts forming at the initial three switching instants and by the reaction front during the fourth cycle are drawn. In this way a step-wise constant approximation for the temperature profile at any instant of the fourth cycle is obtained; (a), (c) schematic representation; (b), (d) comparison between the structure computed based on the algorithm presented in appendix and numerical results.

the contrary may be not true. In particular, symmetric spatiotemporal patterns observed at switch time values fulfilling (10) may exhibit, for some p values, purely thermal fronts reaching the NTW outlet section after a number of cycles lower than $(p - 1)$. Two examples illustrating this possibility are reported in Figure 10. In Figure 10a, values $n_s = 3$ and $N = 4$ are considered. The substitution of p=6 in (10) gives, in this case, switch time values slightly greater than $\tau \cong mod(n_s{\cdot}p,\ N)/(n_s{\cdot}p) = 2/(6V_{th})$. Under these conditions, purely thermal fronts reach, however, the NTW outlet section after a time interval ranging between two and three cycles. Hence, a train of three and not six temperature waves is found. Analogously, Figure 10b shows that, with $n_s = 1$ and $N = 4$, spatiotemporal patterns observed at switch time values fulfilling (10) with $p = 2$ and $p = 3$ exhibit purely thermal fronts intercepting the NTW outlet section after less than one cycle. Accordingly, a temperature profile composed of a single and not two or three temperature waves is observed.

Situations of the type described in Figure 10 may arise when the integers p and $q = mod(n_s{\cdot}p, N)$ have common divisors. If this is the case and switch time values fulfilling (10) are selected, purely thermal fronts can intercept the NTW outlet section within a time interval ranging between $(p'$-1) and p' cycles, with $p' = p/gcd(p, q)$, after covering a number of reactor $q' = q/gcd(p, q)$. Also, the switch time range computed by substituting the selected p in (10) is, in this case, a subdomain of the entire switch time range of existence of symmetric spatiotemporal patterns characterized by p' temperature waves. The whole switch time range must be rather computed by substituting p' and not p in (10). Let us indeed consider the example described in Figure 10a. Substituting $p = 6$ in (10) gives, for such example, the switch time range $\tau \in [mod(3{\cdot}6, 4)/(6V_{th}), mod(3{\cdot}6, 4)/(V_{fr} + 5V_{th})] \equiv [2/(6V_{th}), 2/(V_{fr} + 5V_{th})]$. As previously shown, spatiotemporal patterns characterized by $p' = p/gcd(p, q) = 6/2 = 3$ temperature waves are here found. However, substituting $p' = 3$ in (10) gives the switch time range $\tau \in [mod(3{\cdot}3, 4)/(6V_{th}), mod(3{\cdot}6, 4)/(V_{fr} + 5V_{th})] \equiv [1/(3V_{th}), 1/(V_{fr} + 2V_{th})]$. The upper limit of such range is greater than that found when $p = 6$ is used in (10), while the same lower limit is detected.

Remark 3

It is remarkable to note that the choice $n_s = 1$ adopted in Figure 10b corresponds to the most extensively studied NTW switching strategy. Figure 10b, indeed, shows that, with $N = 4$, this strategy cannot, for example, generate spatiotemporal temperature patterns characterized by two and three temperature waves. These results can be also extended to any N. It can be, in particular, checked that the selection of $n_s = 1$ prevents, in general, the possibility to form spatiotemporal temperature patterns with $p = 1,\ldots, (N - 1)$. Moreover, spatiotemporal patterns characterized by multiple temperature waves can only form, with this strategy, at switch time values $\tau < 1/(N - 1)V_{th}$. On the contrary, the selection of n_s values greater than the unity can allow, at significantly larger switch time values, for the formation of spatiotemporal patterns characterized by a number of temperature waves ranging between 1 and $N - 1$. This happens, for example, with the values $n_s = 3$ considered in Figure 10a. Unlike the case $n_s = 1$, spatiotemporal patterns characterized by numbers of temperature waves $p = 1,\ldots, (N - 1)$ can be obtained here.

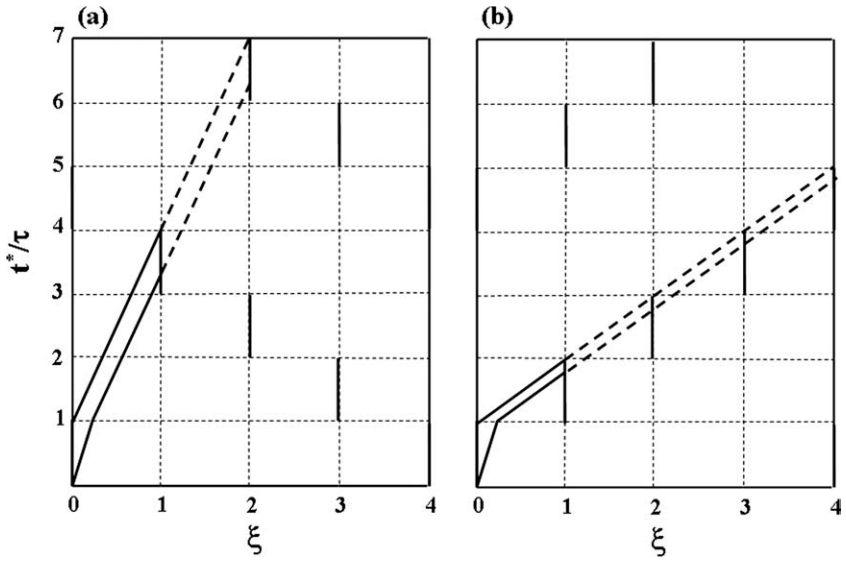

Figure 10. Schematic representation illustrating the impossibility for purely temperature fronts to intercept the NTW outlet section after an arbitrary number of switches.

(a) with n_s =3 and $N = 4$, it is impossible for purely thermal fronts to intercept the NTW outlet section between five and six cycles; (b) $n_s = 1$ and $N = 4$ prevent the possibility to intercept the NTW outlet section during the following three cycles.

Comparison of the Approximate Solution with Numerical Simulation Results

To evaluate the reliability of the derived analytical predictions, projections onto the τ-B plane of the domains of existence of different symmetric T-periodic regimes computed by numerical simulation are compared in Figure 11 with those predicted by inequalities (10). As representative example, the case $N = 5$ and $n_s = 4$ is here considered and periodic regimes corresponding to spatiotemporal patterns characterized by two, three and four temperature waves are analyzed. In accordance with inequalities (10), these regimes are expected to arise over the switch time ranges $[3/(2V_{th}), 3/(V_{th}+V_{fr})]$, $[2/(3V_{th}), 2/(2V_{th}+V_{fr})]$ and $[1/(4V_{th}), 1/(3V_{th}+V_{fr})]$, respectively. The lower limits of such ranges only depend on the purely thermal front velocity $V_{th} = 1/Le$ and are constant as B varies. On the contrary, increasing B produces a reduction of the reaction front velocity V_{fr} shifting to larger switch time values the upper bounds of these ranges.

It is apparent from Figure 11 that the limits predicted based on inequalities (10) include large part of the domains of existence of the considered regimes. Nonetheless, deviations from the predictions of inequalities (10) are found. A non zero adiabatic temperature rise value B^* is detected under which the considered regimes vanish, while switch time ranges of existence of these regimes are predicted, in accordance with inequalities (10), at any nonzero B. Larger B^* values are found as the number p of waves characterizing the temperature pattern increases. Further deviations from analytical predictions are also observed as B is increased. The switch time ranges of existence of the considered regimes always include, indeed, those predicted based on inequalities (10) as B is increased from values slightly greater than B^*. In particular, the lower and the upper limits of existence of the considered regimes predicted based on inequalities (10) result, at such B values, greater and lower than the corresponding limits computed by numerical simulations respectively. Therefore, three different areas of the τ-B plane of existence of the considered regimes are distinguished. These regions are denoted as (i)–(iii) in Figure 11. Region (i) results from the intersection of the domains of existence computed by numerical simulation and those predicted based on inequalities (10) while region (ii) and (iii) represent regions of existence not predicted by (10). It must finally noted that the observed deviations are reduced as Pe_h is increased.

To characterize the physical mechanisms responsible for the observed deviations, it is worth to remark that inequalities (10) have been derived under the assumption of reaction and purely thermal fronts separating cold and hot bed regions. This is equivalent to assume infinitely steep reaction and purely thermal fronts. The fulfillment of these conditions requires, however, the achievement of infinitely large Peclet numbers and reaction rates. If this is not the case, temperature fronts cannot retain a step-like profile and are smoothed due, for example, to the effect of thermal dispersion. Under these conditions, temperature waves traveling over the catalytic bed get deformed since heat is transferred by thermal dispersion to the neighboring cold regions. This effect is clearly described in Figure 12. We here report a comparison of the temperature profiles predicted for the regimes considered in Figure 11 by application of the algorithm presented in appendix and by numerical simulation. The comparison is extended to both the Pe_h values considered in Figure 11. All the displayed profiles are obtained with $B = 3.5$ while switch time values are selected so as to ensure B and τ to lie over regions (i) of Figure 11.

It can be noted that the proposed algorithm satisfactorily describes the qualitative structure of the temperature profile. Nonetheless, temperature waves are significantly smoothed loosing their rectangular-like shape at low Pe_h values. It is

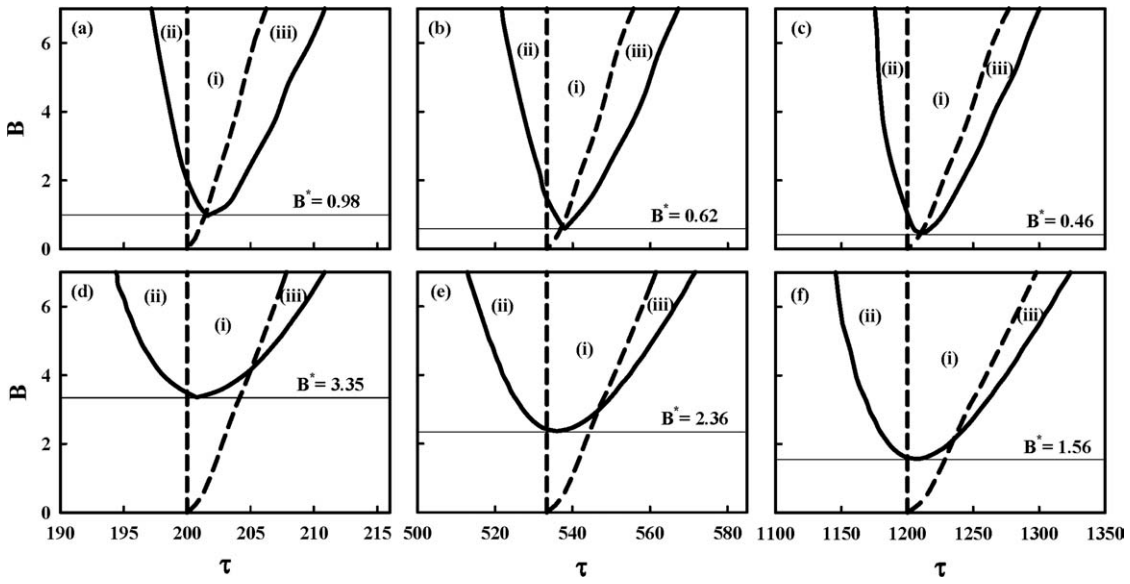

Figure 11. Comparison between the domains of existence of travelling temperature wave trains computed by numerical simulation (solid line) and based on inequalities (10) (dashed line) at Pe_h = 500 ((a), (b), (c)) and Pe_h = 125 ((d), (e), (f)).

Domains of spatiotemporal patterns characterized by 4, 3, and 2 temperature waves are, respectively, displayed in Figures (a) and (d), (b) and (e), (c) and (f).

important to stress that no significant difference is found between the reaction front velocity values observed with the two considered Pe_h values. In particular, $V_{fr} \cong 1/860$ and $V_{fr} \cong 1/876$ at $Pe_h = 100$ and $Pe_h = 500$, respectively. As a result, the widths of the cold and hot bed regions observed with a given number of temperature waves are identical for the two considered Pe_h values. Therefore, the differences observed in Figure 12 between the temperature profiles computed at the same switch time but at the different Pe_h values can be only imputed to variations of the effect of thermal dispersion.

It should be clear, based on the previous analysis, that the analysis of NTW energy balance presented in the third section is not longer valid as the effect of thermal dispersion becomes important. Under these conditions, heat is, indeed, transferred by thermal dispersion to the cold bed regions delimitated by purely thermal fronts making possible to trap the reaction heat within the bed even at switch time values different than those predicted based on inequalities (10). A detailed analysis of the effect of thermal dispersion on the formation of temperature patterns goes, however, beyond the scope of this paper. We consider, rather, appropriate to leave such analysis as the subject of future work.

Conclusions

In this article, the mechanisms governing the emergence of symmetric periodic regimes corresponding to travelling temperature wave-trains in NTWs of N identical catalytic reactors with periodically switched inlet and outlet sections have been investigated for first-order irreversible exothermic reactions. Switching strategies with inlet and outlet sections periodically jumping n_s reactor units have been considered and the effect of varying n_s and the number N of reactors composing the NTW on the stability and the structure of these spatiotemporal patterns have been analyzed. Starting from the analysis of spatiotemporal patterns arising at switching to thermal front velocity ratios around the unity, a geometric approach to the analysis of the NTW energy balance has been developed. Based on this approach, it has been demonstrated that symmetric T-periodic autothermal operation of the NTW can be achieved if purely thermal fronts reach the NTW outlet section after the same number of switches. Following this idea, infinite domains of symmetric periodic regimes corresponding to travelling temperature wave trains have been predicted for any n_s and N. Analytical relationships including the dependence on n_s and N have been derived for the stability limits of the predicted regimes (see inequalities (10) and (11)). Moreover, an algorithm has been developed enabling to get a description for the structure of the corresponding NTW spatiotemporal patterns (see Appendix).

Based on the illustrated geometric approach, it has been also proved that trains characterized by a given number of temperature waves cannot be generated by any switching strategy that is with any n_s. Results presented in this context show, for example, that the most considered switching strategy corresponding to $n_s = 1$ cannot sustain the formation of temperature wave trains with number of waves ranging between 2 and $N - 1$. These results are of great practical importance as they provide guidelines on how to select n_s values guaranteeing the existence of temperature wave trains with desired characteristics.

A comparison between analytical predictions and results of numerical simulation has been finally presented. It has been shown, in this way, that the stability limits predicted based on the derived relationships cover large part of the domains of travelling temperature wave trains computed by numerical simulation. Moreover, good agreement between the structure of NTW spatiotemporal patterns computed by numerical simulation and that predicted based on the proposed algorithm has been found. In this framework, deviations of analytical predictions from the results of numerical

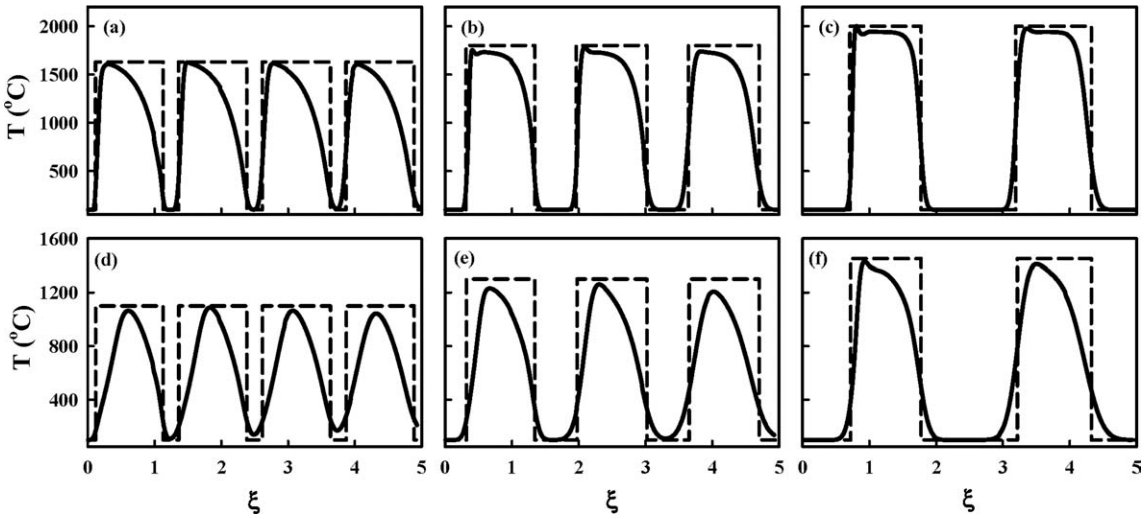

Figure 12. Comparison between temperature and conversion profiles observed in regions (i) of Figures 11a–f (solid line) and their structure derived based on algorithm illustrated in appendix (dashed line) (profiles are computed at $t^* = \tau/2$).

simulations have been analyzed. Particularly, a nonzero adiabatic temperature rise B value has been invariably detected under which temperature wave trains vanish, while switch time ranges of stability of these patterns have been predicted at any nonzero B. The minimum B value enabling the formation of temperature wave trains has been also found to increase at lower Pe_h values. In accordance with these results, only part of the temperature wave trains predicted by the proposed geometric approach can be detected at any set of reactor parameter values as the switch time varies. On the other hand, each predicted temperature wave train can be actually generated by increasing B and/or Pe_h. It is worth to remark, in this context, that the greatest part of the predicted temperature wave trains could be hardly detected by numerical simulation without the knowledge of the appropriate switch time range. If the selected switch time does not belong to this range, extinguished solutions will be indeed found no matter the selected B and Pe_h.

Although the rational application of the presented results will be the subject of forthcoming papers, it is, in our perspective, appropriate to conclude that the presented analysis provides valuable tools to the design and operation of the forced NTW. Particularly, the results presented in this paper prove that appropriately orchestrating the way inlet and outlet NTW sections are switched, desired temperature and concentration patterns can be imposed. Temperature wave trains with desired characteristics can be, indeed, generated. This may have a dramatic impact on process optimization and control as, for example, equilibrium limited reactions and/or complex reaction networks are considered.

Notation

A = Arrhenius constant
B = dimensionless adiabatic temperature rise
c_p = heat capacity
C = concentration
Da = Damköhler number
D_f = mass axial dispersion coefficient
E = activation energy
$f(t)$ = forcing function
$g(t)$ = step-wise constant function defined by Eq. 4
k_e = solid phase axial heat conductivity
L = reactor length
L_0 = NTW length
n_s = number of reactors jumped by inlet and outlet sections
N = number of reactors composing the NTW
Pe = Peclet number
R = gas constant
r = reaction rate
t = time
t^* = dimensionless time
T = temperature °C
u = gas rate
v = dimensionless gas rate
V_{fr} = dimensionless reaction front velocity
V_{sw} = dimensionless switching velocity
V_{th} = dimensionless purely thermal front velocity
x = conversion
z = axial coordinate

Greek letters

γ = dimensionless activation energy
ΔH = heat of reaction
ε = reactor void fraction
θ = dimensionless temperature
ρ = density
τ = dimensionless switch time
ξ = dimensionless axial coordinate

Subscripts and superscripts

0 = reference conditions
f = fluid
h = enthalpy
in = inlet
m = mass

Literature Cited

1. Hoyle R. *Pattern Formation: An Introduction to Methods*. New York: Cambridge University Press, 2006.
2. Wolff J, Papathanasiou AG, Kevrekidis IG, Rotermund HH, Ertl G. Spatiotemporal addressing of surface activity. *Science*. 2001;294:134.
3. Wolff J, Papathanasiou AG, Rotermund HH, Ertl G, Li X, Kevrekidis IG. Gentle dragging of reaction waves. *Phys Rev Lett*. 2003;90:018302.

4. Eigenberger G, Kolios G, Nieken U. Thermal pattern formation and process intensification in chemical reaction engineering. *Chem Eng Sci*. 2007;62:4825.
5. Papathanasiou AG, Wolff J, Kevrekidis IG, Rotermund HH, Ertl G. Some twists and turns in the path of improving surface activity. *Chem Phys Lett*. 2002;358:407.
6. Matros YS. *Catalytic Process Under Unsteady State Conditions*. Amsterdam: Elsevier, 1989.
7. Matros YS, Bunimovich GA. Reverse-flow operation in fixed bed catalytic reactors. *Catal Rev Sci Eng*. 1996;38:1.
8. Haynes TN, Caram HS. The simulated moving bed chemical reactor. *Chem Eng Sci*. 1994;49:5465.
9. Brinkmann M, Barresi AA, Vanni M, Baldi G. Unsteady state treatment of a very lean waste gases in a network of catalytic burners. *Catal Today*. 1999;47:263.
10. Sheintuch M, Nekhamkina O. Comparison of flow-reversal, internal-recirculation and loop reactors. *Chem Eng Sci*. 2004;59:4065.
11. Kolios G, Frauhammer J, Eigenberger G. Autothermal fixed bed reactor concepts. *Chem Eng Sci*. 2000;55:5945.
12. Madai AY, Sheintuch M. Demonstration of loop reactor operation. *AIChE J*. 2008;54:2413.
13. Sheintuch M, Nekhamkina O. The asymptotes of loop reactors. *AIChE J*. 2005;51:224.
14. Russo L, Altimari P, Mancusi E, Maffettone PL, Crescitelli S. Complex dynamics and spatiotemporal patterns in a network of three distributed chemical reactors with periodical feed switching. *Chaos Solitons Fractals*. 2006;28:682.
15. Russo L, Mancusi E, Maffettone PL, Crescitelli S. Symmetry properties and bifurcation analysis of a class of periodically forced reactors. *Chem Eng Sci*. 2002;57:5065.
16. Nekhamkina O, Sheintuch M. Structure of operating domains of loop reactors. *AIChE J*. 2008;54:1292.
17. Mancusi E, Altimari P, Crescitelli S, Russo L. Temperature and conversion patterns in a network of catalytic reactors for methanol synthesis with different switch strategies. *Chem Eng Sci*. 2010;65:4579.
18. Mancusi E, Russo L, Altimari P, Maffettone PL, Crescitelli S. Effect of the switch strategy on the stability of reactor networks. *Ind Eng Chem Res*. 2007;46:6510.
19. Koshy T. *Elementary Number Theory With Applications*. Amsterdam: Elsevier, 2007.
20. Altimari P, Maffetone PL, Crescitelli S, Russo L, Mancusi E. Nonlinear dynamics of a VOC combustion loop reactor. *AIChE J*. 2006;52:2812.

Appendix

Ideas illustrated in the fourth section can be exploited to derive the structure of the NTW spatiotemporal pattern. To this aim, it is sufficient to note that the motion of a temperature front traveling at velocity V and with axial position $\xi = \xi_0$ at $t = 0$ is described by $\xi(t) = mod(\xi_0 + Vt^*, N)$ as far as the front does not reach the NTW outlet section. The latter condition, indeed, corresponds to the extinction of the front. An approximate description for the NTW temperature profile at any $t \in [p\tau, (p+1)\tau]$ can be then derived by the following algorithm:

(1) Compute the positions $\{\chi_1,\ldots,\chi_{2p}\}$ of the purely thermal fronts at switching as follows:

$$\begin{aligned} \chi_{2i-1} &= mod(\xi_{0,i} + V_{\text{th}}(p-i), N), \quad i = 1,\ldots,p \\ \chi_{2i} &= mod(\xi_{0,i} + V_{\text{fr}}\tau + V_{\text{th}}(p-i)\tau, N), \quad i = 1,\ldots,p \end{aligned} \tag{A1}$$

where $\xi_{0,i} = mod(n_s\cdot(p - 2i + N), N)$ denotes the position of the NTW inlet section at the switching instant $(p - i)\tau$.

(2) Arrange the computed sequence $\{\chi_1,\ldots,\chi_{2p}\}$ in increasing order and store the result in the sequence $\{\zeta_{0,1},\ldots,\zeta_{0,2p}\}$.

(3) Compute the positions of purely thermal fronts at $t \in [(p\tau, (p+1)\ \tau]$.as $\{\zeta_1,\ldots, \zeta_{2p}\} = \{\zeta_{0,1} + V_{th}\ (t - p\tau)),\ldots, \zeta_{0,2p} + V_{th}(t - p\tau)\}$

4 Compute the following approximation for the NTW temperature profile at t:

$$T(\xi,t) = T_{\text{in}}(1 + \Delta T_{\max}) \times \left[\Pi\left(\frac{\xi - \frac{(\zeta_{\text{fr}}+\zeta_1)}{2}}{(\zeta_1 - \zeta_{\text{fr}})}\right) + \sum_{i=1}^{p}\Pi\left(\frac{\xi - \frac{(\zeta_{2i}+\zeta_{2i+1})}{2}}{(\zeta_{2i+1} - \zeta_{2i})}\right)\right] \tag{A2}$$

where $\zeta_{\text{fr}} = V_{\text{fr}}\tau$ is the axial position of the reaction front and $\Pi((\xi - b)/c)$ denotes the rectangle function with center c and full-width b.

Note that we have here assumed that the position of the NTW inlet section at $t = p\tau$ is $\xi = 0$. The evolution of the NTW conversion profile during a given cycle can be also approximated, under the formulated assumption, to a unit step function forming immediately after the NTW inlet section and moving over the catalytic bed at constant velocity V_{fr}.

Manuscript received Apr. 3, 2010, and revision received Feb. 10, 2011.